ISSN 1063-7761, Journal of Experimental and Theoretical Physics, 2014, Vol. 118, No. 1, pp. 111–123. © Pleiades Publishing, Inc., 2014.
Original Russian Text © M.N. Popova, E.P. Chukalina, B.Z. Malkin, D.A. Erofeev, L.N. Bezmaternykh, I.A. Gudim, 2014, published in Zhurnal Eksperimental'noi i Teoreticheskoi Fiziki, 2014, Vol. 145, No. 1, pp. 128–142.

ORDER, DISORDER, AND PHASE TRANSITION IN CONDENSED SYSTEM

Crystal Field and Exchange Interactions in the $SmFe_3(BO_3)_4$ Multiferroic

M. N. Popova[a,*], E. P. Chukalina[a], B. Z. Malkin[b], D. A. Erofeev[a,c], L. N. Bezmaternykh[d], and I. A. Gudim[d]

[a] *Institute of Spectroscopy, Russian Academy of Sciences, Troitsk, Moscow, 142190 Russia*
**e-mail: popova@isan.troitsk.ru*
[b] *Kazan (Privolzhsky) Federal University, Kazan, 420008 Russia*
[c] *Moscow Institute of Physics and Technology (State University), Dolgoprudny, Moscow oblast, 141700 Russia*
[d] *Kirenskii Institute of Physics, Siberian Branch, Russian Academy of Sciences, Krasnoyarsk, 660036 Russia*

Received July 5, 2013

Abstract—The optical spectra of oriented $SmFe_3(BO_3)_4$ single crystals are studied in the region of the f–f transitions in the Sm^{3+} ion by Fourier spectroscopy. The energies, the symmetry properties, and the exchange splittings of the Stark sublevels of the ground and 17 excited multiplets of the Sm^{3+} ion in a crystal field of symmetry D_3 are determined from the measured temperature dependences of polarized-radiation absorption spectra. The parameters of the crystal field acting on samarium ions and the parameters of the exchange interaction between Sm^{3+} and Fe^{3+} ions are found. The anisotropy of the effective exchange interaction is shown to be substantially stronger than the magnetic anisotropy, due to a strong crystal-field–induced mixing of the ground and excited multiplets.

DOI: 10.1134/S1063776114010142

1. INTRODUCTION

The study of spectral, magnetic, magnetoelectric, and magnetoelastic properties of multiferroics is of interest for the development of fundamental physics and from a standpoint of possible applications of compounds with coexisting internal electric and magnetic fields in spintronics and optoelectronics. Samarium ferroborate stands out among the compounds from the family of new $RFe_3(BO_3)_4$ (R = Y, La–Lu) multiferroics, since it is the only compound in which spontaneous electric polarization exists in a magnetically ordered phase. Note that, like neodymium ferroborate, $SmFe_3(BO_3)_4$ has the maximum magnetically induced electric polarization (about 500 $\mu C/m^2$) in the row of rare-earth (RE) ferroborates [1, 2].

Samarium ferroborate crystallizes in the trigonal system and has the space group $R32$ [3–5]. This structure remains unchanged down to 2 K [6, 7]. Sm^{3+} ions are surrounded by six O^{2-} ions, which form a trigonal prism with an axis of symmetry located along crystallographic axis c, and occupy the only position with point symmetry group D_3. The measurements of the temperature dependence of magnetic susceptibility [1] and the spectroscopic investigation of oriented $SmFe_3(BO_3)_4$ single crystals [6] showed that the moments of Fe^{3+} ions become ordered in the ab plane, which is normal to the c axis of the crystal, below $T_N = 33$ K. The easy-plane character of the antiferromagnetic structure forming at temperatures $T < T_N$ was supported in neutron scattering experiments performed on $SmFe_3(BO_3)_4$ powders [7]. It was found that the unit cell doubles along the c axis (propagation vector $\mathbf{k} = [0, 0, 3/2]$).

The magnetic moments of iron (samarium) ions are parallel in each crystallographic plane parallel to basal plane ab and are antiparallel in the neighboring nearest planes. The magnetic moments of iron and samarium ions obtained in [7] from an analysis of neutron diffraction data on the assumption of all collinear moments are $4.2\mu_B$ and $0.24\mu_B$, where μ_B is the Bohr magneton, at a temperature of 1.7 K. Note that the version of a magnetic structure with noncollinear magnetic moments of iron and samarium ions, which was also considered in [7], should be rejected, since the magnetic moment of samarium ions found for this structure ($0.8\mu_B$) exceeds the maximum possible value $\mu_B g_J J = (5/7)\mu_B$ in the ground multiplet $^6H_{5/2}$ with Landé factor $g_J = 2/7$ and a full angular momentum $J = 5/2$. Although the question of the orientation of magnetic moments in the ab plane is still open, we can assume that the domains appearing at $T < T_N$ differ in the orientation of collinear magnetic moments of iron and samarium ions along one of the three possible directions of crystallographic axis a, as in a $NdFe_3(BO_3)_4$ crystal [8].

The magnetic properties of $SmFe_3(BO_3)_4$ were studied in [9]. The measured dependences of magnetization on the magnitude and direction of an applied

magnetic field at temperatures above and below T_N were used to determine the parameters of exchange interactions between iron ions and iron and samarium ions in terms of the molecular-field approximation.

$SmFe_3(BO_3)_4$ and $NdFe_3(BO_3)_4$ are the only ferroborates with a purely easy-plane magnetic structure where the component of magnetic moment along the axis c is absent [7]. To explain this circumstance (in particular, as noted in [7]), it is important to know the crystal field parameters, the structure of the wavefunctions of various states of an RE ion in the crystal field, and the parameters of exchange interaction between RE and iron ions. These parameters can be obtained from an analysis of spectroscopic data.

The purpose of this work is to experimentally and theoretically study the Stark structure of the multiplets of the Sm^{3+} ion in $SmFe_3(BO_3)_4$ crystals and the effect of magnetic ordering on the energy spectrum. The obtained results are used to describe the magnetic properties of samarium ferroborate.

2. EXPERIMENTAL

$SmFe_3(BO_3)_4$ single crystals were grown by the solution–melt method using bismuth trimolybdate, i.e., 80 wt % ($Bi_2Mo_3O_{12}$ + $2B_2O_3$ + $0.6Sm_2O_3$) + 20 wt % $SmFe_3(BO_3)_4$. The saturation temperature of this flux (960°C) was determined using probe crystals.

After homogenization at $T = 1050$°C, a ring crystal holder with ten seed crystals 1.0–1.5 mm in size was hung over the flux. The temperature was then decreased to the saturation temperature $T = T_{sat} + 10$°C = 970°C (for the crystal layer damaged in hanging to be melted). At this temperature, the holder with the seed crystals was immersed in the flux and was then rotated at a rate of 30 rpm. After 15 min, the temperature was decreased to $T = T_{sat} - 7$°C = 953°C. The crystals were then grown during a computer-assisted decrease in the temperature at an increasing rate of 1–3 K/day, which ensured a crystal growth rate of at most 1 mm/day (otherwise, defects caused by the trapping of the flux can form). After the end of crystal growth, the holder was lifted above the flux and the furnace was cooled to room temperature at a rate of 50–70 K/h.

The grown single crystals were $5 \times 4 \times 3$ mm^3 in size and had a good optical quality, green color characteristic of ferroborates, and natural faceting. Oriented plates were cut from the single crystals, ground to a thickness of 0.15 mm, and polished. The samples were oriented using crystal morphology and a conoscopic picture. The transmission spectra of the oriented $SmFe_3(BO_3)_4$ single crystals were recorded with a Bruker IFS 125HR Fourier spectrometer in the spectral region 1000–23000 cm^{-1}. A sample was placed in a Cryomech ST403 closed-cycle cryostat at temperatures from 5 to 300 K stabilized at an accuracy of ±0.05 K. The measurements were carried out on plates with the normal parallel to the c axis ($\mathbf{k} \parallel \mathbf{c}$, $\mathbf{E}, \mathbf{H} \perp \mathbf{c}$; α polarization) using nonpolarized light and on samples the plane of which contained the c axis ($\mathbf{k} \perp \mathbf{c}$) in two possible configurations, i.e., $\mathbf{E} \parallel \mathbf{c}$ (π polarization) and $\mathbf{E} \perp \mathbf{c}$ (σ polarization), using linearly polarized light. To increase the signal/noise ratio when recording spectra in the region 16 000–23 000 cm^{-1}, we used an SZS-21 blue–green light filter.

3. EXPERIMENTAL RESULTS

3.1. Transmission and Absorption Spectra of $SmFe_3(BO_3)_4$ Single Crystals in the Paramagnetic Phase

Figure 1 shows the transmission spectrum of a $SmFe_3(BO_3)_4$ single crystal over the entire spectral region (hereafter, ν is the wavenumber) at room temperature. The spectrum has narrow lines, which correspond to the optical f–f transitions between the energy levels of the $4f^5$ electron shell of the Sm^{3+} ion, and broad bands, which are caused by the d–d transitions in Fe^{3+} ions with the $3d^5$ electron shell. The absorption bands corresponding to the transitions of the Fe^{3+} ion from the ground state ^6S to the sublevels of term ^4G split in the crystal field determine the green color of RE ferroborate single crystals. The intense absorption at wavenumbers higher than 24000 cm^{-1} is caused by the transitions of Fe^{3+} ions to charge-transfer states [10].

In a trigonal crystal field, the $^{2S+1}L_J$ multiplets of the Sm^{3+} ion are split into $(2J + 1)/2$ doublets, which transform according to two-valued irreducible representations Γ_4 and Γ_{56} of point symmetry group D_3. Figure 2 shows the absorption spectrum of paramagnetic $SmFe_3(BO_3)_4$ ($T > T_N$) at a sufficiently low temperature (where the transitions from the excited Stark levels of ground multiplet $^6H_{5/2}$ do not manifest themselves) in the region of the $^6H_{5/2} \longrightarrow {}^6H_{13/2}$ transitions in the Sm^{3+} ion for three different polarizations. The seven detected lines reflect the Stark structure of the $^6H_{13/2}$ multiplet. To interpret the absorption spectra of the oriented $SmFe_3(BO_3)_4$ samples recorded with polarized light, we have to take into account the selection rules for electric dipole (ED) and magnetic dipole (MD) transitions in the case of point symmetry group D_3 (Table 1). The coincidence of the α- and σ-polarized spectra in Fig. 2 indicates an ED character of the transitions from the ground state to the levels of the $^6H_{13/2}$ multiplet. The $^6H_{13/2}$ is split into five Γ_4 and two Γ_{56} levels in the crystal field of symmetry D_3 (Table 2).

According to the selection rules for ED transitions, we find that two transitions in π polarization are forbidden in the $^6H_{13/2}$ optical multiplet in the case of the Γ_4 symmetry of the ground state and the other five lines can be observed for all polarizations. In the case of the Γ_{56} symmetry of the ground state, five lines should be absent in π polarization and two lines should be absent in α and σ polarizations. The experimental spectrum corresponds to the Γ_4 symmetry of the

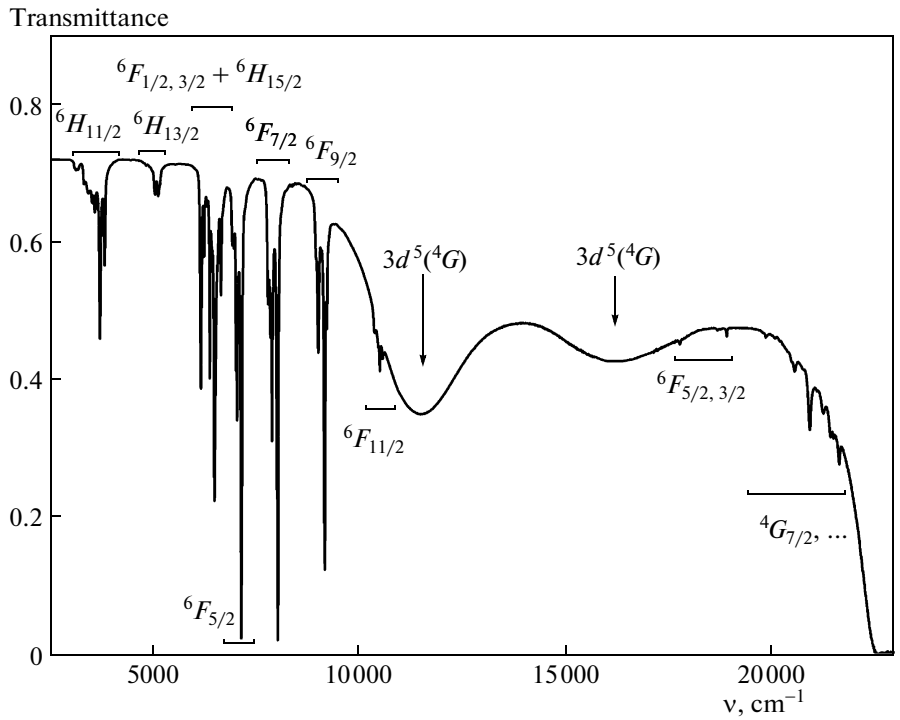

Fig. 1. Transmission spectrum of a $SmFe_3(BO_3)_4$ crystal at room temperature. The final states are indicated for the optical transitions from the levels of the ground $^6H_{5/2}$ multiplet in the Sm^{3+} ions and from the ground ^6S state in the Fe^{3+} ions.

ground state (Fig. 2). With the selection rules, we find the irreducible representations that determine the symmetry properties of the wavefunctions of the Stark levels in the $^6H_{13/2}$ multiplet. They are indicated in Fig. 2 and Table 2 (near the Stark sublevel energies). By analyzing other optical multiplets, we obtained the data given in the second column in Table 2. It should be noted that the $^6H_{5/2}(\Gamma_4(\mathrm{I})) \longrightarrow {}^6H_{7/2}(\Gamma_{56}(\mathrm{C}))$ absorption line has a doublet structure with a splitting of about 11 cm^{-1}, which can be caused by the quasi-resonance interaction of electron excitation ($E_{\mathrm{th}}(\Gamma_{56}(C) = 1183$ cm^{-1}) with lattice vibrations (the vibration frequencies of BO_3 complexes fall in the range 1195–1260 cm^{-1} [11]).

We studied spectra at various temperatures to find the Stark structure of the ground multiplet, which is necessary to interpret the magnetic and thermodynamic properties of $SmFe_3(BO_3)_4$. Figure 3 shows the absorption spectra in the $^6H_{5/2} \longrightarrow {}^6F_{7/2}$ transition region in σ and π polarizations at $T > T_{\mathrm{N}}$ (40 K) and the α-polarization absorption spectra at temperatures well above T_{N}. Figure 4 shows the schematic diagram of the levels that explains the designations of spectral lines. As the temperature decreases, the intensities of the spectral lines corresponding to the transitions from the excited Stark levels of the $^6H_{5/2}$ ground multiplet decrease, since the level population decreases with decreasing temperature. By analyzing the temperature dependences of the "frozen" absorption line intensities with allowance for the distances from the principal spectral lines, we determined the Stark level energies of the $^6H_{5/2}$ ground multiplet (0, 135, 220 cm^{-1}), which turned out to coincide with the preliminary data in [6]. The position of saturated spectral lines I*A*, I*B*, and I*C* was determined by comparing the σ- and π-polarized transmission spectra (Fig. 3). It should be noted that the determined energies and symmetries of the Stark levels of the lower ^6H_J ($J = 5/2$, 7/2, 9/2, 11/2) multiplets agree with the corresponding spectral characteristics of the Sm^{3+} ions substituting for the Y^{3+} ions in an isostructural $YAl_3(BO_3)_4$ crystal [12] (see Table 2).

Table 1. Selection rules for ED and MD transitions in an ion with an odd number of electrons at the site with point symmetry group D_3

D_3	ED		MD	
	Γ_4	Γ_{56}	Γ_4	Γ_{56}
Γ_4	d_x, d_y, d_z α, σ, π	d_x, d_y α, σ	μ_x, μ_y, μ_z α, σ, π	μ_x, μ_y α, π
Γ_{56}	d_x, d_y α, σ	d_z π	μ_x, μ_y α, π	μ_z σ

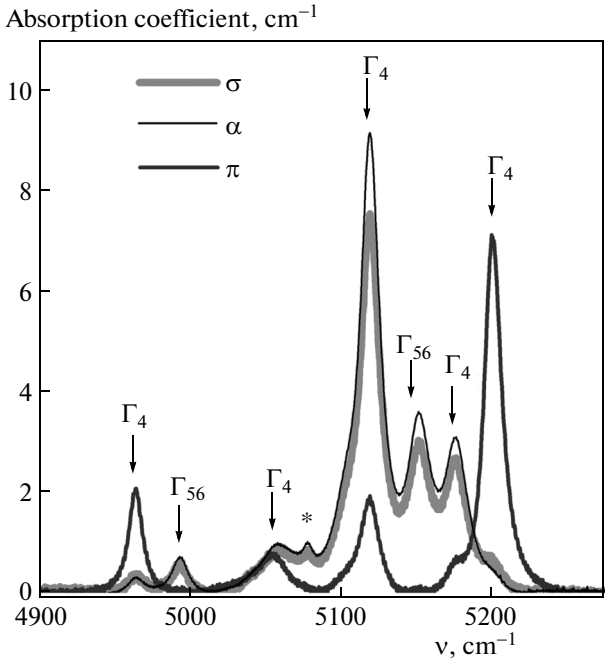

Fig. 2. Absorption spectrum of $SmFe_3(BO_3)_4$ in the region of the ${}^6H_{5/2} \longrightarrow {}^6H_{13/2}$ transition in the Sm^{3+} ion at a temperature of 40 K in σ, α, and π polarization. The asterisk indicates the absorption line of an impurity.

3.2. Spectra of $SmFe_3(BO_3)_4$ in the Magnetically Ordered Phase

Below magnetic ordering temperature $T_N = 33$ K [1, 5–7], the double Kramers degeneracy of energy levels in the crystal field is removed by the exchange interaction of samarium ions with iron ions, the magnetic moments of which are arranged in the planes normal to the *c* axis. Each level splits into two sublevels, and the spectral lines split into four components in the general case (see the schematic diagram in Fig. 4). An example of such a splitting of a spectral line into four components was given in Fig. 1 in [6]. When analyzing the temperature-dependent structure of this line, which corresponds to the ${}^6H_{5/2}(\Gamma_4(\mathrm{I})) \longrightarrow {}^6H_{15/2} + {}^6F_{1/2} + {}^6F_{3/2}(\Gamma_4(C))$ optical transition, at $T < T_N$, we determined the exchange spittings of the ground state ($\Delta_0 = 13.2$ cm^{-1}) and the excited state ($\Delta = 6.7$ cm^{-1}) at 1.7 K.

Figure 5 shows another example of the splitting of a spectral line during the magnetic ordering of an $SmFe_3(BO_3)_4$ crystal in the ${}^6H_{5/2} \longrightarrow {}^6F_{11/2}$ optical multiplet range. Let us trace the shape of the lowest multiplet line (I*A*), ${}^6H_{5/2}(\Gamma_4(\mathrm{I})) \longrightarrow {}^6F_{11/2}(\Gamma_4(A))$, which has the maximum intensity, is not overlapped by other lines, and is not broadened by the phonon-stimulated transitions from the excited state to lower levels. The line splits into two components, the intensity of the low-frequency component decreases, and the distance between the components increases with decreasing temperature. At a temperature of 5 K, this distance is 13.3 ± 0.3 cm^{-1}, which almost coincides with the splitting of the ground doublet of the samarium ion. Thus, the splitting of the $\Gamma_4(A)$ level in the ${}^6F_{11/2}$ multiplet does not exceed 0.6 cm^{-1} and is smaller than the half-widths of the split components.

The wavefunctions of the Γ_{56} symmetry doublets are linear combinations of the states corresponding to the $J_z = \pm 3/2 \pm 3n$ (n is an integer) projections of the total angular momentum onto axis *c*. In spite of the fact that the transverse component of the corresponding *g* tensor is zero, the Γ_{56} doublets in an easy-plane ferromagnet can be split by the exchange field due to mixing with Γ_4 doublets, and this field removes the selection rules considered above (in particular, the exclusion of the $\Gamma_4 \longrightarrow \Gamma_{56}$ ED transitions in π-polarized spectra). The corresponding lines forbidden in the paramagnetic phase can appear in low-temperature spectra if Γ_4 and Γ_{56} are closely spaced. In particular, additional lines appear at temperatures below 20 K in the short-wavelength region of the π-polarized ${}^6H_{5/2} \longrightarrow {}^6F_{11/2}$ absorption spectrum (see Fig. 5). A similar optical magnetoelectric effect of the appearance of forbidden lines in a magnetically ordered phase was observed earlier in the spectrum of the easy-axis $PrFe_3(BO_3)_4$ antiferromagnet in [13]. The exchange-induced splittings in the measured spectra of $SmFe_3(BO_3)_4$ were detected for two doublets, namely, $\Gamma_{56}(E)$ in multiplet ${}^6F_{9/2}$ and $\Gamma_{56}(B)$ in multiplet ${}^6F_{11/2}$ (see Table 2).

In Fig. 6, we compare the temperature dependences of the exchange splitting of line I*A* (considered above) in the optical multiplet ${}^6H_{5/2} \longrightarrow {}^6F_{11/2}$ and the magnetic moment of the iron ion in $SmFe_3(BO_3)_4$ measured by neutron scattering [7]. (Note that a similar comparison was performed in [6] with the data on $YFe_3(BO_3)_4$, which has a slightly different structure, because of unavailable neutron diffraction data on $SmFe_3(BO_3)_4$ at that time.) The fact that the temperature dependence of the splitting of the spectral line of the Sm^{3+} ion is proportional to the magnetic moment of the iron ion indicates the predominant contribution of the Sm–Fe exchange interaction to the "exchange field" acting on samarium ions. The interaction between samarium ions is very weak, since SmO_6 prisms are isolated from each other because of the crystal structure of ferroborates and, hence, do not have common oxygen ions.

Thus, the splitting of the levels of the Sm^{3+} ion is mainly determined by the interaction with the iron subsystem. Table 2 gives the exchange splittings

$$\Delta_{\mathrm{exp}}(j) = E_+(j, T = 5\ \mathrm{K}) - E_-(j, T = 5\ \mathrm{K}) \qquad (1)$$

found from an analysis of the low-temperature spectra and the shifts of the centers of gravity of some Stark sublevels (j) of excited multiplets with respect to the

Table 2. Energy levels of the Sm^{3+} ion in the paramagnetic phase of a $SmFe_3(BO_3)_4$ crystal obtained from an experiment (E_{exp} [cm^{-1}], $T = 40$ K) and a calculation (E_{th} [cm^{-1}]). The energy levels of the Sm^{3+} ion in $YAl_3(BO_3)_4$ are given in parentheses [12]. The exchange splittings of the Kramers doublets determined from low-temperature spectra (Δ_{exp} [cm^{-1}], $T = 5$ K) and a calculation (Δ_{th} [cm^{-1}]). Calculated g factors. Exchange interaction–induced shifts of the centers of gravity of the doublets obtained from an experiment (δE_{exp} [cm^{-1}], $T = 5$ K) and a calculation (δE_{th} [cm^{-1}])

$^{2S+1}L_J$	E_{exp}			E_{th}	Δ_{exp}	Δ_{th}	$g_\perp$	$g_\parallel$	δE_{exp}	δE_{th}
$^6H_{5/2}$	0		Γ_4I	0	13.2	13.16	0.679	0.491	0	0
$(2\Gamma_4 + \Gamma_{56})$	135	(136)	Γ_{56}II	135.5	–	0.03	0	1.63	–	0.36
	220	(194)	Γ_4III	219.3	–	0.74	0.03	1.47	–	0.53
$^6H_{7/2}$	1091	(1081)	Γ_4A	1084.9	6.8	3.49	2.30	0.51	1.0	0.23
$(3\Gamma_4 + \Gamma_{56})$	1115	(1132)	Γ_4B	1122.3	<1	0.50	0.23	2.47	2.9	0.33
	1173	(1183)	$\Gamma_{56}C$	1182.9	0	0	0	2.34	–	0.42
	1184									
	–	(1282)		1286.8	–	2.09	0.85	5.15	–	0.35
$^6H_{9/2}$	2296	(2293)	Γ_4A	2298.5	2	1.00	3.97	2.47	0.4	0.32
$(3\Gamma_4 + 2\Gamma_{56})$	2321	(2323)	Γ_4B	2326.6	2.4	2.04	3.03	1.72	2.0	0.33
	–	(2354)	$\Gamma_{56}C$	2353.2	0	0	0	2.95	–	0.36
	2404	(2408)	Γ_4D	2399.4	–	1.81	4.13	0.92	–	0.36
	2509	(2496)	$\Gamma_{56}E$	2500	–	0	0	9.31	–	0.35
$^6H_{11/2}$	–	(3616)		3605.5	–	6.37	7.0	1.09	–	0.08
$(4\Gamma_4 + 2\Gamma_{56})$	–	(3648)		3645.3	–	0.06	0	2.10	–	0.17
	–			3670.3	–	6.49	6.03	0.94	–	0.73
	3716	(3713)	Γ_{56}	3710.6	<2	0.17	0	9.36	2.9	–0.13
	3729	(3738)		3727.9	–	6.01	5.96	3.47	–	0.84
	3835	(3808)	Γ_4	3821.3	0	0.02	0.02	13.0	3.8	0.4
$^6H_{13/2}$	4964		Γ_4A	4965.7	15	10.84	8.78	1.23	0.9	–0.56
$(5\Gamma_4 + 2\Gamma_{56})$	4994		$\Gamma_{56}B$	4999.5	0	0.25	0	3.74	1.1	0.75
	5055		Γ_4C	5057.4	–	4.02	2.91	5.81	–	0.46
	5119		Γ_4D	5119.4	2	3.54	2.82	8.28	0.7	–0.01
	5152		$\Gamma_{56}E$	5152.6	0	0.05	0	11.3	1.4	0.23
	5178		Γ_4F	5174.8	<1	0.59	0.46	13.9	2.4	0.63
	5203		Γ_4G	5190	<1	0.67	0.52	16.3	3.4	0.97
$^6H_{15/2}$	6333		Γ_4A	6337.2	13	14.4	10.2	0.91	0.4	–1.27
$(5\Gamma_4 + 3\Gamma_{56})$	–		B	6372.6	–	0.69	0	4.30	–	1.08
$^6F_{1/2}(\Gamma_4)$	6372		Γ_4C	6388.1	6.7	7.76	0.36	1.33	1.5	0.05
	–		D	6436.5	–	4.38	2.96	5.15	–	0.69
	6518		Γ_4E	6526.8	10	3.94	2.77	8.00	3.4	–0.19
	6543			6534.8	<2	0.31	0	18.5	3.4	1.02
	6626			6634.5	–	2.36	0	9.49	–1.9	–0.92
$^6F_{3/2}\Gamma_4$	6626		Γ_4	6634.6	–	2.50	2.83	1.24	4.4	1.44
$^6F_{3/2}\Gamma_{56}$	6649			6657.3	0	0.03	0	5.67	2.9	0.40
	–			6716.4	–	1.18	0.80	13.8	–	–0.19
	–			6742.8	–	1.17	0.75	16.6	–	1.53
$^6F_{5/2}$	7133		Γ_{56}	7122.1	0	0.02	0	3.91	1.2	0.18
$(2\Gamma_4 + \Gamma_{56})$	7148		Γ_4	7149.5	<2	2.02	1.08	4.05	–0.1	0.38
	7174		Γ_4	7183.4	4	5.51	3.12	0.48	1.9	0.54

Table 2. (Contd.)

$^{2S+1}L_J$	E_{exp}		E_{th}	Δ_{exp}	Δ_{th}	$g_\perp$	$g_\parallel$	δE_{exp}	δE_{th}
$^6F_{7/2}$	7982	$\Gamma_4 A$	7972.6	5.4	4.73	2.84	4.07	1.4	–0.32
$(3\Gamma_4 + \Gamma_{56})$	8000	$\Gamma_{56} B$	7996.4	0	0.20	0	4.39	1.4	0.46
	8021	$\Gamma_4 C$	8016	4.7	3.86	2.18	5.65	1.4	0.65
	8052	$\Gamma_4 D$	8067.8	6.6	8.57	4.96	2.73	1.1	0.64
$^6F_{9/2}$	9146	$\Gamma_4 A$	9136.9	4.2	3.59	2.22	8.97	–1.6	–0.64
$(3\Gamma_4 + 2\Gamma_{56})$	9158	$\Gamma_{56} B$	9165.9	0	0	0	11.6	1.4	0.73
	9191	$\Gamma_4 C$	9186.1	7.6	5.07	2.99	4.80	0.9	–0.32
	9211	$\Gamma_4 D$	9218.3	5.5	6.84	6.38	0.02	–3.5	–3.69
	9213	$\Gamma_{56} E$	9214.4	4.6	4.57	0	3.91	5.9	5.69
$^6F_{11/2}$	10489	$\Gamma_4 A$	10477	0	0.02	0.01	15.8	–0.6	0.17
$(4\Gamma_4 + 2\Gamma_{56})$	10554	$\Gamma_{56} B$	10561	1.4	5.94	0	8.13	–2.6	–6.15
	10565	$\Gamma_4 C$	10557	10.5	9.31	8.31	1.93	3.8	5.88
	10589	$\Gamma_4 D$	10599	–	2.31	3.49	5.67	–	–5.88
	10592	$\Gamma_{56} E$	10602	–	1.43	0	9.24	–	2.09
	10599	$\Gamma_4 F$	10612	7	4.53	3.84	7.98	8.9	6.03
$^4F_{5/2}$	17785	Γ_{56}	17784	0	0	0	2.21	0.4	0.27
$(2\Gamma_4 + \Gamma_{56})$	17901		17874	–	3.22	2.0	0.04	1.4	0.38
	18113		18091	–	1.10	0.28	3.16	2.4	0.33
$^4F_{3/2}$	18879	Γ_4	18867	9	6.46	0.88	0.39	–0.1	–0.26
$(\Gamma_4 + \Gamma_{56})$	18898	Γ_{56}	18884	0	0.23	0	1.50	2.1	0.96
$^4G_{7/2}$	19972		19962	1.3	0.55	1.63	3.54	0	0.33
$(3\Gamma_4 + \Gamma_{56})$	19993		20001	0	0	0	3.09	0.4	0.34
	20017		20029	–	0.87	2.24	0.21	0.4	0.35
	20212		20199	–	0.15	0.35	6.89	–0.1	0.34
$^4I_{9/2}$	–		20388	–	7.84	3.38	1.09	–	–0.21
$(3\Gamma_4 + 2\Gamma_{56})$	–		20410	–	0.18	0	6.37	–	0.74
$^4M_{15/2}$	20482		20497	0	0.01	0	8.26	0.4	0.24
$(5\Gamma_4 + 3\Gamma_{56})$	20508.5		20524	11	5.86	3.63	0.18	1.4	0.44
	20549		20535	0	0.41	0	5.43	1.4	0.20
	20599		20580	–	0.10	1.97	1.80	–	0.18
	20615		20618	–	0.04	0.44	5.08	–	0.49
	20670		20661	–	2.05	0	3.17	–	0.15
	–		20675	–	1.64	2.16	6.16	–	0.12
	20695		20683	–	0.94	2.25	3.79	–	0.83
	–		20823	–	0.81	0.88	6.96	–	0.22
	20872		20860	–	0.01	1.32	6.38	–	0.17
	20909		20873	–	–	0	7.19	–	0.60
$^4I_{11/2}$	–		20972	–	2.78	4.63	0.24	–	0.30
$(4\Gamma_4 + 2\Gamma_{56})$	21019		21016	–	0	0	2.54	–	0.32
$^4I_{13/2}$	–		21045	–	1.19	2.72	0.03	–	0.36
$(5\Gamma_4 + 2\Gamma_{56})$	21088		21092	–	1.25	2.87	1.02	–	0.33
	–		21103	–	0.67	0.85	5.41	–	0.36
	21160		21161	0	0	0	8.22	–	0.34
	–		21472	–	0.53	6.32	0.45	–	0.34

Table 2. (Contd.)

$^{2S+1}L_J$	E_{exp}	E_{th}	Δ_{exp}	Δ_{th}	$g_\perp$	$g_\parallel$	δE_{exp}	δE_{th}
	–	21478	–	0	0	2.51	–	0.38
	–	21494	–	0.63	5.38	0.24	–	0.37
	21543	21523	–	0.38	2.42	8.97	–	0.38
	–	21556	–	0.47	2.78	7.11	–	0.31
	–	21567	–	0	0	8.17	–	0.27
	21619	21575	–	0.14	0.54	10.6	–	0.54
$^4K_{15/2}$	22142	22120	0	1.26	1.66	2.06	0.4	0.33
$(5\Gamma_4 + 3\Gamma_{56})$	22167	22156	3	0.54	1.25	4.07	0.9	0.34
$^4M_{17/2}$	22188	22200	0	0	0	3.09	1.4	0.35
$(6\Gamma_4 + 3\Gamma_{56})$	22293	22298	–	0.05	0.02	14.0	–	0.34
$^4G_{5/2}$	–	22402	–	0	0	13.5	–	0.33
$(2\Gamma_4 + \Gamma_{56})$	–	22456	–	0.40	7.53	2.79	–	0.33
$^4G_{9/2}$	–	22480	–	0	0	3.98	–	0.30
$(3\Gamma_4 + 2\Gamma_{56})$	–	22481	–	0.29	6.35	0.51	–	0.37
	22491	22489	–	0.26	7.07	1.84	–	0.33
	22592	22597	–	0.90	4.34	6.10	–	0.30
	–	22602	–	0	0	8.06	–	0.33
	–	22611	–	0.17	4.48	5.95	–	0.34
	–	22746	–	0.04	0	4.12	–	0.01
	–	22762	–	1.49	2.98	4.1	–	0.49
	–	22772	–	4.63	5.53	0.54	–	0.51
	–	22815	–	3.11	5.45	3.50	–	0.26
	–	22829	–	3.37	5.19	4.77	–	0.20
	–	22841	–	0.07	0	7.36	–	0.53
	–	22870	–	0	0	9.59	–	0.36
	–	22896	–	0.52	1.07	5.65	–	0.37
	–	22913	–	0	0	12.5	–	0.36
	–	22940	–	0.42	0.81	8.78	–	0.43
	–	23038	–	0.02	0	9.70	–	0.11
	–	23048	–	2.40	5.97	0.42	–	0.52
	–	23052	–	2.53	6.06	0.55	–	0.49

center of gravity of the ground doublet ($j = 1$) in comparison with the corresponding energies in the paramagnetic phase,

$$\delta E_{exp}(j) = \frac{1}{2}[E_+(j, T = 5\text{ K}) + E_-(j, T = 5\text{ K})] - \frac{1}{2}[E_+(1, T = 5\text{ K}) + E_-(1, T = 5\text{ K})] - E(j, T = 40\text{ K}). \quad (2)$$

Here, E_+ and E_- are the energies of the upper and lower components of the split doublet, respectively.

4. THEORETICAL ANALYSIS OF THE STARK STRUCTURE AND THE EXCHANGE SPLITTINGS

To analyze the measured energy spectrum of the Sm^{3+} ions in the paramagnetic $SmFe_3(BO_3)_4$ phase, we used the Hamiltonian

$$H = H_{FI} + H_{CF}, \quad (3)$$

where H_{FI} is the effective Hamiltonian of the free Sm^{3+} ion and H_{CF} is the Hamiltonian corresponding to the interaction of the ground electron configuration of the Sm^{3+} ion ($4f^5$) with the crystal field. In the free-ion

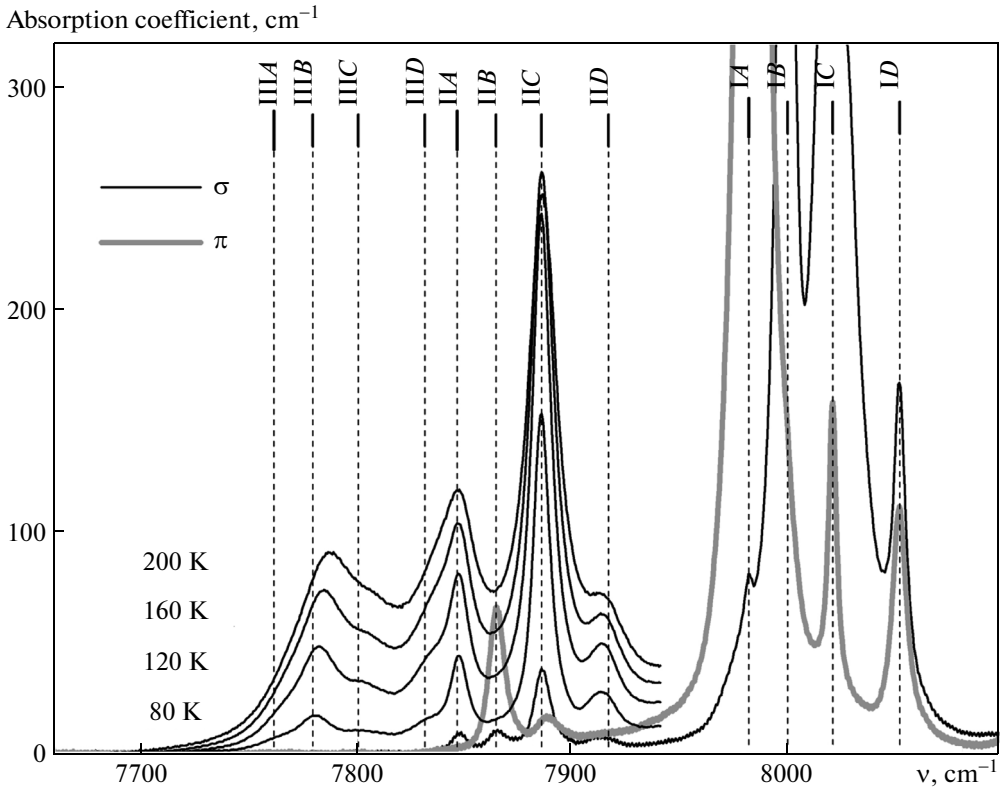

Fig. 3. Absorption spectra of $SmFe_3(BO_3)_4$ in σ and π polarization at a temperature of 40 K in the region of the $^6H_{5/2} \longrightarrow {}^6F_{7/2}$ transition in the Sm^{3+} ion. Low-frequency region, the α-polarization absorption spectra at high temperatures that correspond to the transitions from the excited Stark levels of the ground $^6H_{5/2}$ multiplet in the Sm^{3+} ion.

Hamiltonian presented in the standard form [14, 15], we took into account the electrostatic interaction between 4*f* electrons, which is determined by Slater parameters $F^2 = 78876$ cm^{-1}, $F^4 = 56633$ cm^{-1}, and $F^6 = 40002$ cm^{-1}; spin–orbit interaction with a coupling constant $\xi = 1167$ cm^{-1}; the two- and three-particle terms corresponding to the interaction between various electron configurations with parameters $\alpha = 20.16$, $\beta = -567$, $\gamma = 1500$, $P^2 = 357$, $P^4 = 268$, $P^6 = 178$, $T^2 = 304$, $T^3 = 36$, $T^4 = 56$, $T^6 = -347$, $T^7 = 373$, and $T^8 = 348$; and additional relativistic terms with parameters $M^0 = 2.6$, $M^2 = 1.46$, and $M^4 = 0.81$ (in cm^{-1}). These parameters and the crystal field parameters given below were found by comparing the eigenvalues of the Hamiltonian (3) with the measured energy levels of samarium ions in the range $E_{exp} < 20300$ cm^{-1} (see Table 2). In the Cartesian coordinate system with axes *z* and *x* directed along crystallographic axes *c* and *a* (axis of symmetry C_2), respectively, the crystal field at the positions of Sm^{3+} ions with point symmetry D_3 can be described by six independent parameters B_q^p ($p = 2, 4, 6$; $p \geq q = 0, -3, 6$),

$$H_{CF} = \sum_k [B_0^2 C_0^{(2)}(k) + B_0^4 C_0^{(4)}(k) + iB_{-3}^4 (C_{-3}^{(4)}(k) + C_3^{(4)}(k)) + B_0^6 C_0^{(6)}(k) + iB_{-3}^6 (C_{-3}^{(6)}(k) + C_3^{(6)}(k)) + B_6^6 (C_6^{(6)}(k) + C_{-6}^{(6)}(k))]. \quad (4)$$

The sum in Eq. (4) is taken over all 4*f* electrons, and $C_q^{(p)}(k)$ is the one-electron spherical tensor operator of rank *p*. As the initial set of parameters of the Hamiltonian (3) in the variational simulation of the measured spectrum, we used the free-ion parameters from [15] and the crystal field parameters presented for the Nd^{3+} ions in a $NdFe_3(BO_3)_4$ crystal in [16].

It should be noted that the diagonalization of Hamiltonian (3) was performed using the full basis of the $4f^5$ configuration, which contains 2002 Slater determinants constructed from one-electron functions. The crystal field parameters obtained in this work are compared with the corresponding parameters of isostructural RE compounds (see Table 3). This comparison points to a monotonic relation between the crystal field parameters and the number of elec-

trons N in the unfilled 4f shell, namely, the decrease in the absolute values of B_q^p in the series of RE ferroborates from praseodymium ($N = 2$) to terbium ($N = 8$) that is caused by the compression of the electron shell with increasing N.

The crystal field parameters found in this work differ substantially from the parameters used in [9] to describe the magnetic properties of $SmFe_3(BO_3)_4$ with allowance for the states of only ground multiplet $^6H_{5/2}$ and from the parameters obtained in [12] for impurity samarium ions in $YAl_3(BO_3)_4$. (In particular, the different signs of parameters B_{-3}^4 and B_{-3}^6 in [12] are in conflict with the lattice structure, which deprives these parameters of physical meaning.) The parameters of the quadrupole component of crystal field B_0^2 in [9, 12] are approximately half the value required to obtain the calculated splitting of the $^4F_{3/2}$ multiplet to be compared with the measurement data.

The calculated energies E_{th} of the Stark sublevels of most multiplets agree satisfactorily with the experimental data (see Table 2). It should be noted that the qualitative difference between the calculated and measured Stark structures of the $^6F_{9/2}$ and $^6F_{11/2}$ multiplets (closely spaced sublevels $\Gamma_{56}(E)$ and $\Gamma_4(D)$ in multiplet $^6F_{9/2}$ and sublevels $\Gamma_{56}(B)$ and $\Gamma_4(C)$ in multiplet $^6F_{11/2}$ change over in the calculated spectrum) can be caused by the additional shifts of the RE ion energy levels in the crystal field that are induced by both electron–phonon interaction and the anisotropic interactions between 4f electrons [19], which was not taken into account in this work. At high energies (above 20900 cm^{-1}), the detected lines cannot be unambiguously identified because of a high density of the levels in the calculated spectrum that belong to overlapping multiplets.

The splitting of an isolated Kramers doublet in external magnetic field **B** is determined by the eigenvalues of an effective spin Hamiltonian ($S = 1/2$); in the case of axial symmetry, it has the form

$$H_S = \mu_B g_\perp (S_x B_x + S_y B_y) + \mu_B g_\parallel S_z B_z.$$

When calculating the matrix elements of the operator components of the magnetic moment of the samarium ion,

$$\boldsymbol{\mu} = -\mu_B \sum_k (\mathbf{l}_k + 2\mathbf{s}_k)$$

(where $\mathbf{l}_k$ and $\mathbf{s}_k$ are the operators of the orbital and spin moments of the kth electron, respectively) using the eigenfunctions of operator (3), we found the trans-

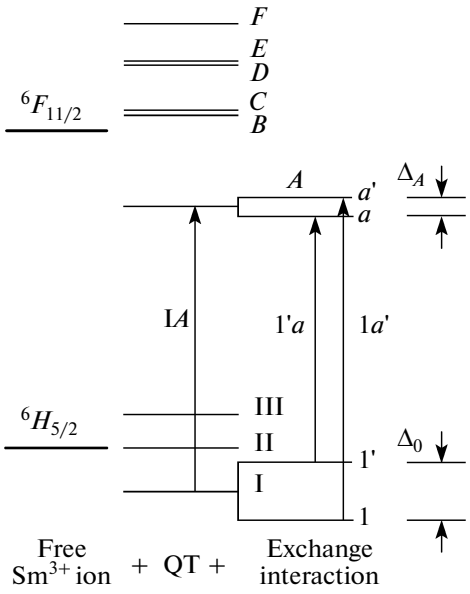

Fig. 4. Schematic diagram of the transitions between the Stark levels of the ground ($^6H_{5/2}$) and excited ($^6F_{11/2}$) multiplets of the Sm^{3+} ion in the crystal field of $SmFe_3(BO_3)_4$ and the exchange splittings of the Kramers doublets in the magnetically ordered state of $SmFe_3(BO_3)_4$.

Table 3. Crystal field parameters in $RM_3(BO_3)_4$ borate crystals with structure type $R32$

p,	q	B_q^p, cm^{-1}					
		$PrFe_3(BO_3)_4$ [17]	$NdFe_3(BO_3)_4$ [16]	$SmFe_3(BO_3)_4$ this work	$SmFe_3(BO_3)_4$ [9]	$YAl_3(BO_3)_4$:Sm^{3+} [12]	$TbFe_3(BO_3)_4$ [18]
2,	0	556	551	502	285	270	464
4,	0	−1447	−1239	−1048	−900	−1569	−1256
4,	−3	867	697	575	1520	890	608
6,	0	534	519	432	–	246	352
6,	−3	165	105	87	–	−480	73
6,	6	376	339	290	–	396	270

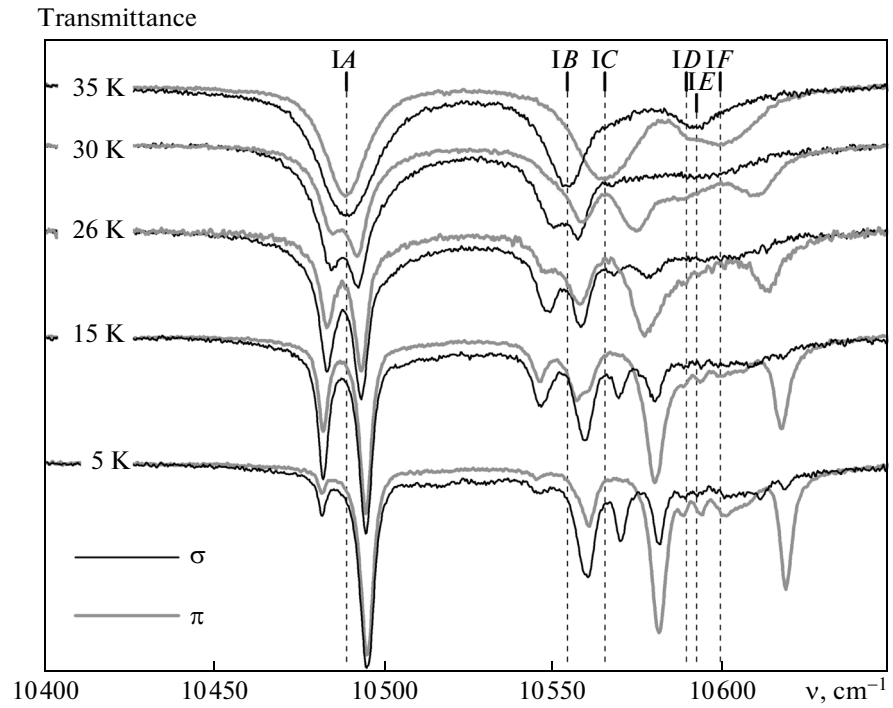

Fig. 5. Transmission spectra of $SmFe_3(BO_3)_4$ in σ and π polarizations at various temperatures in the region of the $^6H_{5/2} \longrightarrow {}^6F_{11/2}$ transition in the Sm^{3+} ion. The appearance of the I*B* line in π-polarization during magnetic ordering is visible.

verse ($g_{xx} = g_{yy} = g_\perp$) and longitudinal ($g_{zz} = g_\parallel$) g factors for each doublet,

$$g_{\alpha\alpha} = \frac{2}{\mu_B}\sqrt{\langle +|\mu_\alpha|+\rangle^2 + \langle +|\mu_\alpha|-\rangle^2}, \qquad (5)$$

where $|+\rangle$ and $|-\rangle$ are the Kramers-conjugate wavefunctions of the given doublet. The results are given in Table 2. Note that the calculated determinant of the g tensor matrix of the ground doublet of the Sm^{3+} ions has a positive value, in contrast to a negative value of this determinant in the case of the ground state of the Nd^{3+} ions in $NdFe_3(BO_3)_4$ [20].

The Hamiltonian of the exchange interaction of the Sm^{3+} ion with the Fe^{3+} ion in the S state with spin $S_{Fe} = 5/2$ can be written as

$$H_{exch} = \mathbf{F}\cdot\mathbf{S}_{Fe},$$

where operator $\mathbf{F}$ acts in the space of the states of the samarium ion and, in the general case, is determined by 28 parameters $a_q^{(p)}$ [21],

$$\mathbf{F} = \sum_{p=0,2,4,6}\sum_{q=-p}^{p}\sum_k a_q^{(p)}C_q^{(p)}(k)\mathbf{s}_k. \qquad (6)$$

Taking into account only the isotropic part of the exchange interaction,

$$H_{is} = -2J_{fd}\mathbf{S}_R\cdot\mathbf{S}_{Fe}$$

(where $\mathbf{S}_R = \sum_k \mathbf{s}_k$ is the operator of the total spin momentum of the Sm^{3+} ion), we can estimate the exchange integral $J_{fd} = -a_0^{(0)}/2$ that determines the exchange interaction of the nearest samarium and iron ions, using the splitting Δ_0 of the ground state of samarium ions measured at a low temperature. We replace the operator of the spin moment of Fe^{3+} ions by the corresponding mean value ($\langle S_{Fe,z}\rangle = \langle S_{Fe,y}\rangle = 0$, $\langle S_{Fe,x}\rangle = \pm 2.1$ [7]) and the operator of the total spin of the Sm^{3+} ion by its project on the states of the doublet (on the assumption of no mixing of the wavefunctions of different multiplets); take into account the six nearest Fe^{3+} ions; and obtain the effective spin Hamiltonian of the samarium ion in the form $H_S = -\Delta_0 S_x$, where

$$|\Delta_0| = 12g_\perp\left|J_{fd}\langle S_{Fe,x}\rangle(1-g_J^{-1})\right|. \qquad (7)$$

When substituting the splitting of the ground doublet ($\Delta_0 = 13.2\ cm^{-1} = 19.1$ K) measured at a temperature of 5 K, Landé splitting factor $g_J = 2/7$, and the calculated g factor ($g_\perp = 0.68$) into Eq. (7), we obtain the exchange integral $J_{fd} = 0.446$ K (the corresponding exchange field is $B_{exch} = \Delta_0/\mu_B g_\perp = 41.9$ T). We obtained a more exact value of the exchange integral ($J_{fd} = 0.345$ K) from an analysis of the spectrum of Sm^{3+} ions in the magnetically ordered phase of a $SmFe_3(BO_3)_4$ crystal, which is based on the calcula-

tion of the eigenvalues of the Hamiltonian of Sm^{3+} ions

$$H_{MP} = H_{FI} + H_{CF} - 12J_{fd}\langle S_{Fe,x}\rangle S_{R,x} \quad (8)$$

in the complete space of the states of the $4f^5$ electron shell. The substantial difference from the initial estimate is caused by a strong mixing of the wavefunctions of the ground ${}^6H_{5/2}$ multiplet and the relatively closely spaced excited ${}^6H_J$ multiplets ($J = 7/2, 9/2, ...$) by the crystal field. As a result of this mixing, the total moment is not a "good" quantum number. The positive sign of the exchange integral corresponds to ferromagnetic ordering of the iron and samarium sublattices in each layer normal to axis c and, correspondingly, to the antiparallel arrangement of the magnetic moments of samarium ions and the nearest iron ions located at the vertices of the regular triangles in the neighboring layers. The found exchange integral agrees well with the f–d exchange interaction parameters obtained earlier for $RFe_3(BO_3)_4$ RE ferroborates: $J_{fd} = 0.513$ K (R = Pr [17]), $J_{fd} = 0.48$ K (R = Nd [16]), and $J_{fd} = 0.26$ K (R = Tb [18]). As the number of electrons in the $4f$ shell increases and its radius decreases, the exchange integral and the crystal field parameters decrease monotonically.

When analyzing the excitation frequencies of $SmFe_3(BO_3)_4$ single crystals measured at temperatures $T < T_N$ in submillimeter transmission spectra, the authors of [20] concluded that the f–d interaction is strongly anisotropic. The dynamic exchange field that acts on samarium ions in the basal plane and is induced by the fluctuations of the spin moments of iron ions is an order of magnitude higher than the exchange field along trigonal axis c [20]. At low temperatures, the effective exchange interaction can be represented by the projection of the operator H_{is} on the states of the ground doublet of samarium ions,

$$H_{is}^{(0)} = -2J_{fd}[G_\perp(S_{Fe,x}S_x + S_{Fe,y}S_y) + G_\parallel S_{Fe,z}S_z]. \quad (9)$$

The components of the "spin" G factor introduced into spin Hamiltonian (9) are determined by relations similar to Eq. (5). We calculated the matrix elements of the operator of the total spin moment of the Sm^{3+} ion in the basis constructed from the eigenfunctions of operator (3) and found $|G_\perp| = 2.2$ and $|G_\parallel| = 0.328$; that is, the exchange anisotropy ($G_\perp/G_\parallel = 6.71$) does exceed the magnetic anisotropy substantially ($g_\perp/g_\parallel = 1.38$).

The splittings Δ_{th} of the Kramers doublets of samarium ions and the exchange-field-induced shifts δE_{th} of their centers of gravity with respect to the center of gravity of the ground doublet that were obtained from the calculation of the eigenvalues of Hamiltonian (8) using the exchange integral and the average iron ion spin given above are compared with the measurement data in Table 2. The nonzero shifts of the doublets are caused by the second-order exchange interaction effects. Since the ground state can move only downward in the energy scale, most values of δE_{th} are positive. The shifts of the order of 1 cm^{-1} are comparable with the error in determining the frequencies of the broad spectral lines. The anomalously large (in absolute value) shifts (more than 1 cm^{-1}) of some neighboring doublets with opposite signs point to a strong mixing of their wavefunctions in the magnetically ordered phase. In particular, we note a strong repulsion of the $\Gamma_{56}(E)$ and $\Gamma_4(D)$ levels in the ${}^6F_{9/2}$ multiplet and also of the $\Gamma_{56}(B)$ and the $\Gamma_4(C)$, $\Gamma_4(D)$ and $\Gamma_{56}(E)$ and $\Gamma_4(F)$ levels in the ${}^6F_{11/2}$ multiplet, which was found from calculations and agree with the measurement results.

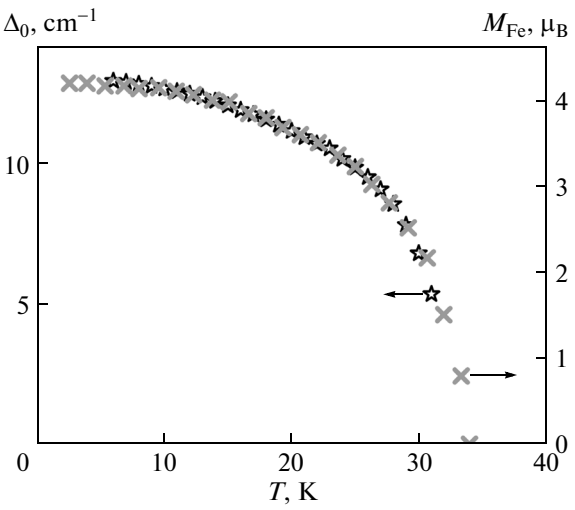

Fig. 6. Temperature dependences of the exchange splitting of the spectral line IA, ${}^6H_{5/2}(\Gamma_4(I)) \longrightarrow {}^6F_{11/2}(\Gamma_4(A))$, in the spectrum of $SmFe_3(BO_3)_4$ and the magnetic moment of iron ions in $SmFe_3(BO_3)_4$ according to the neutron scattering data in [7].

The relationships between the calculated values of splittings Δ_{th} of various doublets during the consideration of only the isotropic component of the exchange interaction with the exchange integral corresponding to the splitting of the ground state agree qualitatively with the experimental data (see Table 2). The difference between the calculated (Δ_{th}) and experimental (Δ_{exp}) values can be decreased by taking into account the anisotropic terms in exchange interaction operator H_{exch}. In particular, the calculation of the splittings with allowance for three nonzero parameters in Eq. (6), namely, $a_0^{(0)} = -0.7$ K, $a_0^{(2)} = 1.45$ K, and $a_0^{(6)} = 6.52$ K, makes it possible to decrease the root-mean-square deviation of the calculated splittings from the measured values from 2.4 to 1.9 cm^{-1} for 20 Stark levels with the maximum measured splittings.

The correspondence between the calculated and measured results is illustrated in Fig. 7: the serial numbers of the doublets for which measured splittings Δ_{exp}

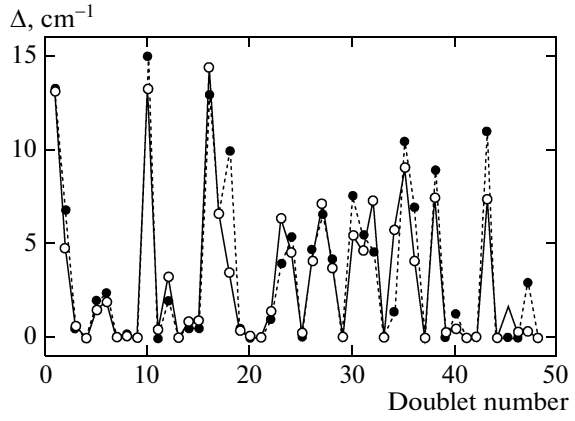

Fig. 7. (●) Measured (Δ_{exp}) and (○) calculated (Δ_{th}) doublet splittings in the spectrum of the Sm^{3+} ion at a temperature of 5 K.

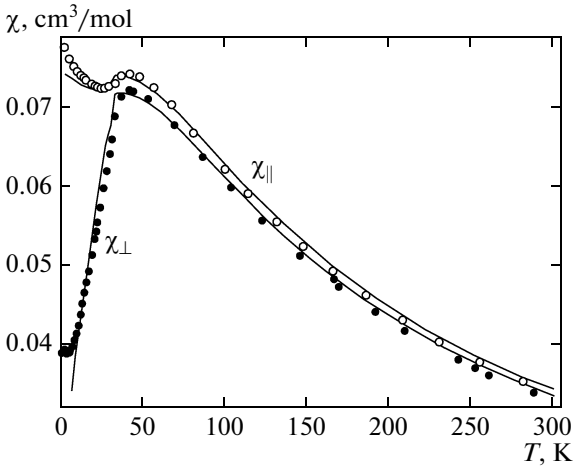

Fig. 8. (solid curves) Calculated temperature dependences of the components of the static magnetic susceptibility tensor of an $SmFe_3(BO_3)_4$ crystal. (symbols) The measurement data from [9].

are given in Table 2 are laid off as abscissa (beginning from the ground state). At present, we have no information (e.g., on spectral changes in external magnetic fields) required to analyze the structure of operator (6) in detail. Nevertheless, it is obvious that the isotropic component of the exchange interaction plays a key role in samarium ferroborate, in contrast to praseodymium ferroborate studied in [17]. This conclusion agrees with the results of analysis of the spectral and magnetic properties of terbium ferroborate, which is based on the consideration of isotropic *f–d* exchange [18]. It should be noted that the calculation of the spectrum of the samarium ion in terms of the model used in [9] to describe the magnetization anisotropy measured at $T = 2$ K in magnetic fields $\mathbf{B} \parallel \mathbf{c}$ and $\mathbf{B} \perp \mathbf{c}$ results in the doublet splittings that differ substantially from the measured ones. (In this calculation, we took info account three nonzero parameters of the exchange interaction operator (6), namely, $a_0^{(0)} < 0$, $a_0^{(2)} = -18.8$ K, and $a_0^{(4)} = 21.7$ K.)

Having determined the parameters of the crystal field and the *f–d* exchange interaction, we can simulate the equilibrium magnetic properties of samarium ferroborate single crystals. We restrict ourselves to the consideration of the temperature dependences of the longitudinal ($\chi_{zz} = \chi_\parallel$) and transverse ($\chi_{xx} = \chi_{yy} = \chi_\perp$) components of magnetic susceptibility tensor of an $SmFe_3(BO_3)_4$ single crystal that were measured in a magnetic field $B = 0.1$ T [1, 9]. The underestimated values of susceptibility $\chi_\parallel$ and, conversely, the overestimated values of $\chi_\perp$ at low temperatures in [1] as compared to the measurement data in [9] are likely to result from an error in the sample orientation. The field-induced magnetization of RE ferroborates contains the contributions of the following two interacting magnetic subsystems: the quasi-one-dimensional subsystem of iron ions, which are coupled with the nearest neighbors in screw chains parallel to axis *c* by antiferromagnetic exchange interaction, and the RE subsystem. The contribution of iron ions can be estimated from the results of studying the characteristics of an $YFe_3(BO_3)_4$ crystal [22], where RE ions were replaced by diamagnetic yttrium ions. However, a detailed comparison of the susceptibilities of $SmFe_3(BO_3)_4$ and $YFe_3(BO_3)_4$ crystals (see Fig. 4 in [9]) is incorrect, since their crystal lattices have different space groups ($R32$ and $P3_121$, respectively) and their magnetic ordering temperatures are different. A higher temperature in $YFe_3(BO_3)_4$ ($T_N = 38$ K) as compared to $SmFe_3(BO_3)_4$ ($T_N = 33$ K) indicates a stronger interaction between iron ions and, correspondingly, a weaker response (lower susceptibility of the Fe^{3+} subsystem) to an external field in yttrium ferroborate. Although the difference between the susceptibilities of the Fe^{3+} subsystems in samarium and yttrium ferroborates is expected to be rather small, it can be comparable with the contribution of samarium ions, which have low *g* factors of the ground multiplet sublevels.

According to the measurement data in [1, 9], the $\chi_\parallel(T)$ curve is slightly above the $\chi_\perp(T)$ curve over the entire temperature range (Fig. 8). The difference between the longitudinal and transverse components of the susceptibility tensor of Sm^{3+} ions is negative, at least at low temperatures ($T < 70$ K), because of the relation $g_\parallel < g_\perp$ between the *g* tensor components of the ground state. Therefore, the positive sign of the measured difference between longitudinal and transverse susceptibilities can only be related to the magnetic anisotropy of iron ions. The susceptibility tensor components calculated in terms of the model developed in [16–18] agree satisfactorily with the experimental data (see Fig. 8). The calculation in this work was performed using the operator of the bilinear anisotropic

exchange interaction between neighboring iron ions in chains,

$$H_{dd} = -2\sum_{\alpha} J_{nn}^{(\alpha\alpha)} S_{\mathrm{Fe1},\alpha} S_{\mathrm{Fe2},\alpha}$$

with parameters $J_{nn}^{(xx)} = J_{nn}^{(yy)} = J_{nn,\perp} = -7$ K and $J_{nn}^{(zz)} = J_{nn,\parallel} = -6.4$ K, in contrast to the operator of isotropic interaction with an exchange integral $J_{nn,\perp} = J_{nn,\parallel} = J_{nn} = -6.25$ K introduced earlier for neodymium [16] and praseodymium [17] ferroborates and with an integral of –6.7 K for terbium ferroborate [18]. Note that the introduced relation between the parameters $|J_{nn,\perp}| > |J_{nn,\parallel}|$ agrees with the observed magnetic structure of samarium ferroborate.

5. CONCLUSIONS

We measured the energies in the paramagnetic and magnetically ordered phases of the $SmFe_3(BO_3)_4$ multiferroic and the exchange splittings in the magnetically ordered phase for the Stark levels of the ground and excited multiplets of the Sm^{3+} ions in an $SmFe_3(BO_3)_4$ crystal and determined the symmetry properties of the corresponding wavefunctions. We also found the parameters of the crystal field acting on the samarium ions and the parameters of the *f–d* exchange interaction between the nearest iron and samarium ions, in which an isotropic component is predominant, and the *d–d* interaction between the nearest iron ions. The anisotropy of the effective exchange interaction was shown to be substantially stronger than the magnetic anisotropy due to a strong mixing of the ground and excited multiplets of samarium ions by the crystal field.

ACKNOWLEDGMENTS

This work was supported by the Russian Foundation for Basic Research (project no. 13-02-00787) and the basic research program Quantum Mesoscopic and Disordered Structures of the Presidium of the Russian Academy of Sciences.

REFERENCES

1. Yu. F. Popov, A. P. Pyatakov, A. M. Kadomtseva, G. P. Vorob'ev, A. K. Zvezdin, A. A. Mukhin, V. Yu. Ivanov, and I. A. Gudim, J. Exp. Theor. Phys. **111** (2), 199 (2010).
2. A. A. Mukhin, G. P. Vorob'ev, V. Yu. Ivanov, A. M. Kadomtseva, A. S. Narizhnaya, A. M. Kuz'menko, Yu. F. Popov, L. N. Bezmaternykh, and I. A. Gudim, JETP Lett. **93** (5), 275 (2011).
3. J. C. Joubert, W. B. White, and R. J. Roy, J. Appl. Crystallogr. **1**, 318 (1968).
4. J. A. Campa, C. Cascales, E. Gutierrez-Puebla, M. A. Monge, I. Rasines, and C. Ruiz-Valero, Chem. Mater. **9**, 237 (1997).
5. Yukio Hinatsu, Yoshihiro Doi, Kentaro Ito, Makoto Wakeshima, and Abdolali Alemi, J. Solid State Chem. **172**, 438 (2003).
6. E. P. Chukalina, M. N. Popova, L. N. Bezmaternykh, and I. A. Gudim, Phys. Lett. A **374**, 1790 (2010).
7. C. Ritter, A. Pankrats, I. Gudim, and A. Vorotynov, J. Phys.: Condens. Matter **24**, 386002 (2012).
8. M. Janoschek, P. Fisher, J. Schefer, B. Roessli, V. Pomjakushin, M. Meven, V. Petricek, G. Petrakovskii, and L. Bezmaternikh, Phys. Rev. B: Condens. Matter **81**, 094429 (2010).
9. A. A. Demidov, D. V. Volkov, I. A. Gudim, E. V. Eremein, and V. L. Temerov, J. Exp. Theor. Phys. **116** (5), 800 (2013).
10. A. M. Kalashnikova, V. V. Pavlov, R. V. Pisarev, L. N. Bezmaternykh, M. Bayer, and Th. Rasing, JETP Lett. **80** (5), 293 (2004).
11. D. Fausti, A. Nugroho, P. H. M. van Loosdrecht, S. A. Klimin, M. N. Popova, and L. N. Bezmaternykh, Phys. Rev. B: Condens. Matter **74**, 024403 (2006).
12. I. Kibaili and M. Dammak, J. Lumin. **132**, 2092 (2012).
13. M. N. Popova, T. N. Stanislavchuk, B. Z. Malkin, and L. N. Bezmaternykh, Phys. Rev. Lett. **102**, 187403 (2009).
14. H. M. Crosswhite and H. Crosswhite, J. Opt. Soc. Am. B **1**, 246 (1984).
15. W. T. Carnall, G. L. Goodman, K. Rajnak, and R. S. Rana, J. Chem. Phys. **90**, 3443 (1989).
16. M. N. Popova, E. P. Chukalina, T. N. Stanislavchuk, B. Z. Malkin, A. R. Zakirov, E. Antic-Fidancev, E. A. Popova, L. N. Bezmaternykh, and V. L. Temerov, Phys. Rev. B: Condens. Matter **75**, 224435 (2007).
17. M. N. Popova, T. N. Stanislavchuk, B. Z. Malkin, and L. N. Bezmaternykh, Phys. Rev. B: Condens. Matter **80**, 195101 (2009).
18. M. N. Popova, T. N. Stanislavchuk, B. Z. Malkin, and L. N. Bezmaternykh, J. Phys.: Condens. Matter **24**, 196002 (2012).
19. B. R. Judd, Phys. Rev. Lett. **39**, 242 (1977).
20. A. M. Kuz'menko, A. A. Mukhin, V. Yu. Ivanov, A. M. Kadomtseva, and L. N. Bezmaternykh, JETP Lett. **94** (4), 294 (2011).
21. P. M. Levy, Phys. Rev. [Sect.] A **135**, 155 (1964).
22. E. A. Popova, A. N. Vasiliev, V. L. Temerov, L. N Bezmaternykh, N. Tristan, R. Klingeler and B. Büchner, J. Phys.: Condens. Matter **22**, 116006 (2010).

Translated by K. Shakhlevich